Theory of size mismatched alloy systems: many-body Kanzaki forces

2008 J. Phys.: Condens. Matter 20 045207

(http://iopscience.iop.org/0953-8984/20/4/045207)

J. Phys.: Condens. Matter **20** (2008) 045207 (9pp) doi:10.1088/0953-8984/20/04/045207

Theory of size mismatched alloy systems: many-body Kanzaki forces

O Shchyglo[1], A Díaz-Ortiz[1], A Udyansky[1], V N Bugaev[1], H Reichert[1], H Dosch[1] and R Drautz[2]

[1] Max-Planck-Institut für Metallforschung, Heisenbergstraße 3, D-70569 Stuttgart, Germany
[2] Department of Materials, University of Oxford, Parks Road, Oxford OX1 3PH, UK

Received 18 July 2007, in final form 1 November 2007
Published 8 January 2008
Online at stacks.iop.org/JPhysCM/20/045207

Abstract

A perturbative approach to determining the strain-induced effective interactions in binary alloys with large atomic size mismatch is presented. Using the chemical energy as the reference state, the strain-induced energy of the alloy is cast into a many-body (Kanzaki) force expansion that depends on both the configurational and displacive degrees of freedom. It is shown that the k-space energy expansion is valid for all wavelengths. The theory is then applied to the Cu_3Au alloy where, due to the large difference between atomic sizes, considerable relaxations are observed from first-principles calculations. We found that the inhomogeneous contribution ($\boldsymbol{k} \neq 0$) dominates the strain energy in Cu_3Au, whereas the homogeneous part ($\boldsymbol{k} = 0$), notwithstanding its configurational dependence, contributes only a few per cent.

1. Introduction

The interdependence between elastic and configurational degrees of freedom plays a fundamental role in the prediction of the configurational energetics and thermodynamics of partially ordered alloys and superlattices with atomic size mismatch. Particularly, the competition between ordering and phase separation in alloys is often controlled by the delicate balance between chemical and elastic interactions, as evidenced by thermodynamic calculations [1–4] and diffuse scattering measurements [5]. Elastic interactions have proven to be all-important in describing the long-period limit in superlattices [2].

It is customary to describe the alloy configurational energy as the sum of elastic, chemical, and relaxation terms [3, 6–10]. The elastic energy part corresponds to the homogeneous lattice distortions. Although in the literature elastic energy is often taken as solely dependent on the atomic concentration [1, 8, 9], in general the atomic configuration also makes significant contribution. The chemical contribution arises from the configurational degrees of freedom, i.e., from placing the different atomic species on the ideal sites of a parent lattice following a pattern $\boldsymbol{\sigma}$ in a given volume Ω. The relaxation term, on the other hand, arises from the energy gain when the atoms relax inhomogeneously towards their equilibrium positions. In this way, the relaxation energy couples the alloy configuration to the displacive degrees of freedom.

The elastic and the relaxation terms, as defined above, belong to a single contribution that complements the chemical part. This *strain-induced* energy is elastic in nature and depends on the configuration $\boldsymbol{\sigma} = \{\sigma_i\}$ and the positions $\boldsymbol{R} = \{\boldsymbol{R}_i\}$ of the atoms,

$$E_{\text{alloy}}(\boldsymbol{\sigma}, \boldsymbol{R}, \Omega) = E_{\text{chem}}(\boldsymbol{\sigma}, \Omega) + E_{\text{strain}}(\boldsymbol{\sigma}, \boldsymbol{R}, \Omega). \quad (1)$$

Herein the equilibrium geometry of the system for a given $\boldsymbol{\sigma}$ is determined by the condition that the (resulting) forces acting on individual sites vanish, i.e.,

$$\boldsymbol{F}_i \equiv -\frac{\partial E_{\text{alloy}}}{\partial \boldsymbol{R}_i} = 0. \quad (2)$$

In general, a given lattice distortion can always be decomposed into its homogeneous and inhomogeneous contributions. This allows the strain-induced energy to be written as

$$E_{\text{strain}} = E^{\text{H}}_{\text{strain}} + E^{\text{I}}_{\text{strain}}. \quad (3)$$

The homogeneous (elastic) contribution $E^{\text{H}}_{\text{strain}}$ accounts for the long-wavelength limit and can be determined by the elastic constants of the alloy (as functions of the atomic concentration and configuration). The inhomogeneous part $E^{\text{I}}_{\text{strain}}$, on the other hand, accounts for the distortion field caused by single atoms ('injection energy'), pairs, triplets and higher order atom clusters in the host lattice. In other words, $E^{\text{I}}_{\text{strain}}$ contains all the many-body strain-induced interactions.

One could treat all energy contributions *implicitly* by cluster expanding E_{alloy} in terms of concentration-independent interactions, as the alloy energy is then described in terms of a complete and orthogonal basis in the configurational space [11, 12]. In fact, the cluster expansion method has been successfully applied to a number of systems with moderate atomic size mismatch [3, 13]. In practice, however, systems with considerable long-ranged strain-induced interactions require the inclusion of virtually infinite terms in the expansion [2, 7, 8, 14, 15]. Most of the previous efforts and advances in understanding the interplay between the strain-induced and chemical (configurational) interactions have considered ad hoc assumptions on the homogeneous and inhomogeneous contributions to E_{strain}. Some first-principles approaches have handled the chemical part within the cluster expansion method, treating the strain-induced contribution via the constituent strain energy in the long-wavelength limit [2, 3].

A rather different approach to the description of the strain-induced interactions in solids is the Kanzaki force formalism [15–17]. The two-body Kanzaki force description of atomic size mismatched alloys has been implemented on a phenomenological level, in which empirical values for the elastic constants and the concentration dependence of the lattice parameters were considered [7, 8, 18, 19]. First-principles electronic structure approaches have also been implemented within this two-body scheme [9, 10]. Many-body strain-induced interactions in alloys, however, have been rarely considered in the literature [15, 20–24]. In particular, neither the dependence of many-body strain-induced interaction on interatomic distances nor the dispersion laws of their Fourier components have been studied within the semi-phenomenological or first-principles theories. These are some of the aims of the present contribution.

In this paper, we present a first-principles microscopic elasticity (k-space) theory within the framework of the Matsubara–Kanzaki–Krivoglaz lattice statics [15–17]. The theory treats both homogeneous (corresponding to the long-wavelength limit $\boldsymbol{k} = 0$) and inhomogeneous ($\boldsymbol{k} \neq 0$) contributions of E_{strain} on the same footing, thus satisfying equation (3) and providing results valid in the entire wavelength range. The strain-induced energy is calculated as a perturbation of the ideal (chemical) state, coupling seamlessly the many-body correlation functions (configurational degrees of freedom) to many-body Kanzaki forces. Within this framework, deviations of Vegard's law arise as a natural consequence of the many-body strain-induced interactions in $E^{\text{H}}_{\text{strain}}$.

The rest of the paper is organized as follows. In section 2 we derive a Kanzaki force formalism that includes the well-known pairwise formulation of the strain-induced interactions and then we expanded the theory to encompass nonlinear effects via many-body interactions. Also an explicit derivation of the two-, three- and four-body strain-induced interactions is given in terms of the lattice Green function. A first-principles parametrization *beyond* pair strain-induced interactions is presented for Cu–25 at.% Au alloys in section 3. We close the paper with our concluding remarks.

2. Theory

2.1. General considerations

In the decorated and undistorted lattice, all atoms sit on the ideal positions $\boldsymbol{R} = \{\boldsymbol{R}_1, \boldsymbol{R}_2, \ldots, \boldsymbol{R}_N\}$ of the parent lattice according to the configuration $\boldsymbol{\sigma} = \{\sigma_{\boldsymbol{R}_1}, \sigma_{\boldsymbol{R}_2}, \ldots, \sigma_{\boldsymbol{R}_N}\}$. This state defines the chemical contribution for which a configurational cluster expansion can be written as

$$E_{\text{chem}} = \sum_{\alpha} V^{\alpha}\sigma_{\alpha}, \qquad \text{with } \sigma_{\alpha} = \prod_{i\in\alpha}\sigma_{\boldsymbol{R}_i}, \tag{4}$$

where $\sigma_{\boldsymbol{R}_i} = 1(0)$ if site $\boldsymbol{R}_i$ is occupied by an A (B) atom. The V^{α} are the effective cluster interactions associated with cluster figure α (= empty cluster, point, pairs, triplets, etc).

The strain-induced energy contribution is defined as a perturbation of the alloy energy—which in the decorated and unperturbed state is equal to E_{chem}—with respect to a set of atomic displacements $\boldsymbol{u}_{\boldsymbol{R}}$ from the ideal positions $\boldsymbol{R}$

$$E_{\text{strain}} = \sum_{\boldsymbol{R}_i} \boldsymbol{u}_{\boldsymbol{R}_i}\left(\frac{\partial E_{\text{alloy}}}{\partial \boldsymbol{u}_{\boldsymbol{R}_i}}\right)_0 + \frac{1}{2}\sum_{\boldsymbol{R}_i,\boldsymbol{R}_j} \boldsymbol{u}^{\text{T}}_{\boldsymbol{R}_j}\left(\frac{\partial^2 E_{\text{alloy}}}{\partial \boldsymbol{u}_{\boldsymbol{R}_i}\partial \boldsymbol{u}_{\boldsymbol{R}_j}}\right)_0 \boldsymbol{u}_{\boldsymbol{R}_i} + \text{O}(3), \tag{5}$$

where the derivatives are evaluated in the undistorted lattice. Expression (5) describes the static strain-induced energy corresponding to an arbitrary atomic displacement field $\{\boldsymbol{u}_{\boldsymbol{R}_i}\}$, including (mechanically) stable and unstable states.

The first term in equation (5) is the work done upon the system when the atoms are displaced by $\boldsymbol{u}_{\boldsymbol{R}}$ away from their ideal lattice positions $\boldsymbol{R}$. The force on the atom located at lattice site i, characterized by σ_i and $\boldsymbol{u}_{\boldsymbol{R}_i}$, is

$$\boldsymbol{\varphi}_{\boldsymbol{R}_i} = -\sum_{\alpha\neq i}\left(\frac{\partial V^{\alpha}}{\partial \boldsymbol{u}_{\boldsymbol{R}_i}}\right)_0 \sigma_{\alpha} = \sum_{\alpha\neq i}\boldsymbol{\varphi}^{\alpha}_{\boldsymbol{R}_i}\sigma_{\alpha}, \tag{6}$$

where $\boldsymbol{\varphi}^{\alpha}_{\boldsymbol{R}_i}$ are the many-body forces associated with a cluster figure α acting on site i. For two-body forces this results in the Kanzaki forces (see below) [17].

The second term in the right-hand side of equation (5) is the potential energy of the distorted lattice, which can conveniently be expressed in terms of the generalized Born–von Karman tensor:

$$\boldsymbol{\Phi}_{\boldsymbol{R}_j,\boldsymbol{R}_i} = \boldsymbol{\Phi}^{(0)}_{\boldsymbol{R}_j,\boldsymbol{R}_i} + \sum_{\alpha\neq i,j}\left(\frac{\partial^2 V^{\alpha}}{\partial \boldsymbol{u}_{\boldsymbol{R}_i}\partial \boldsymbol{u}_{\boldsymbol{R}_j}}\right)_0 \sigma_{\alpha}, = \boldsymbol{\Phi}^{(0)}_{\boldsymbol{R}_j,\boldsymbol{R}_i} + \sum_{\alpha\neq i,j}\boldsymbol{\Phi}^{\alpha}_{\boldsymbol{R}_j,\boldsymbol{R}_i}\sigma_{\alpha}. \tag{7}$$

Using equations (6) and (7), we can write the strain-induced energy as

$$E_{\text{strain}} = -\sum_{\boldsymbol{R}_i}\boldsymbol{\varphi}_{\boldsymbol{R}_i}\boldsymbol{u}_{\boldsymbol{R}_i} + \tfrac{1}{2}\sum_{\boldsymbol{R}_i,\boldsymbol{R}_j}\boldsymbol{u}^{\text{T}}_{\boldsymbol{R}_j}\boldsymbol{\Phi}_{\boldsymbol{R}_j,\boldsymbol{R}_i}\boldsymbol{u}_{\boldsymbol{R}_i}, \tag{8}$$

where $\boldsymbol{\varphi}$ are the generalized Kanzaki forces, i.e., the material's constants that describe how a solute atom (or a defect) distorts the host lattice.

Linear microscopic elasticity theory corresponds to a harmonic approximation, in the $\boldsymbol{u}_{\boldsymbol{R}}$ and $\sigma_{\boldsymbol{R}}$ variables, of equation (8). The superposition approximation is valid in the

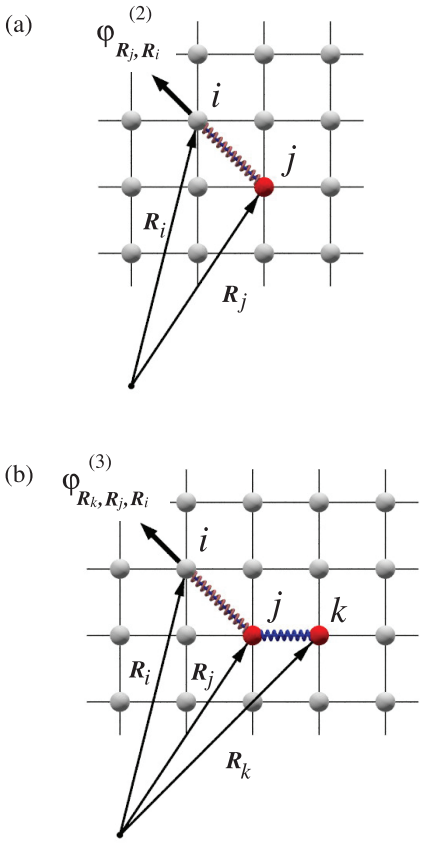

Figure 1. (a) Two-body Kanzaki force on site $\boldsymbol{R}_i$ induced by the atom at site $\boldsymbol{R}_j$. (b) Three-body Kanzaki force on site $\boldsymbol{R}_i$, where the displacement $\boldsymbol{u}_{R_i}$ depends on the configuration and location of sites $\boldsymbol{R}_j$ and $\boldsymbol{R}_k$.

(This figure is in colour only in the electronic version)

harmonic case, i.e., the total distortion generated by a group of solute atoms is the direct sum of the individual distortions of the atoms comprising the group [8]. Going beyond the superposition (harmonic) approximation translates into many-body strain-induced interactions. Anharmonic effects can be first observed in a third-order expansion of equation (8):

$$E_{\text{strain}} \approx \tfrac{1}{2}\sum_{R_i,R_j} \boldsymbol{u}^{\mathrm{T}}_{R_i}\boldsymbol{\Phi}^{(0)}_{R_j,R_i}\boldsymbol{u}_{R_j} - \sum_{R_i,R_j}\boldsymbol{\varphi}^{(2)}_{R_j,R_i}\boldsymbol{u}_{R_i}\sigma_{R_j} - \sum_{R_i,R_j,R_k}\boldsymbol{\varphi}^{(3)}_{R_k,R_j,R_i}\boldsymbol{u}_{R_i}\sigma_{R_j}\sigma_{R_k}. \tag{9}$$

Note that the strain-induced energy has the full rotational and translational symmetry of the crystal structure, therefore the expansion coefficients depend only on differences of the atomic positions, i.e.,

$$\boldsymbol{\varphi}^{(2)}_{R_j,R_i} = \varphi^{(2)}_{R_j,R_i}\frac{\boldsymbol{R}_j-\boldsymbol{R}_i}{|\boldsymbol{R}_j-\boldsymbol{R}_i|} \tag{10}$$

with $\boldsymbol{\varphi}^{(2)}_{R_j,R_i} \equiv \boldsymbol{\varphi}^{(2)}_{R_j-R_i}$ as the force on site $\boldsymbol{R}_i$ induced by the atom at site $\boldsymbol{R}_j$ (figure 1(a)). The three-body Kanzaki forces are written in a similar fashion:

$$\boldsymbol{\varphi}^{(3)}_{R_k,R_j,R_i} = \varphi^{(3)}_{R_k,R_j,R_i}\frac{\boldsymbol{R}_j-\boldsymbol{R}_i}{|\boldsymbol{R}_j-\boldsymbol{R}_i|}, \tag{11}$$

where, as in the case of two-body forces, $\varphi^{(3)}_{R_k,R_j,R_i} \equiv \varphi^{(3)}_{R_j-R_i,R_i-R_k}$. Many-body Kanzaki forces account for the nonlinear effects in elastically inhomogeneous crystals, i.e., the change of the crystal lattice misfit caused by the strain generated in a neighbourhood of the solute atom at site $\boldsymbol{R}_j$. The physical picture corresponds closely to that of a solute atom at site $\boldsymbol{R}_i$ affected by the 'polarization' strain produced in the neighbourhood of an atom sitting on $\boldsymbol{R}_j$. In the case of three-body Kanzaki forces, the lattice misfit (the polarization strain) is caused by the presence of an atom at site $\boldsymbol{R}_k$ (see figure 1(b)). The analogy between the strain-induced interactions and the dipole–dipole interaction of molecules can be taken further: in both cases the absence of polarizability leads to purely pairwise interaction that decays as r^{-3} with separation distance. Similar to van der Waals interaction in molecules, generated by the polarization-induced dipole momentum, the misfit polarization produces many-body interactions [26].

As a last comment on the three-body Kanzaki forces (schematically depicted in figure 1(b)), we note that the direct force contribution on site $\boldsymbol{R}_i$ induced by an atom at $\boldsymbol{R}_k$ is already contained in the second term of the right-hand side of equation (9). By definition, many-body Kanzaki forces associated with a cluster figure α do not contain contributions from any of the subclusters ($\beta \in \alpha$).

2.2. Homogeneous strain energy and Vegard's law

The mechanical state of a crystal lattice can be thought of as the confluence of the two different types of strains. One is the homogeneous strain that describes the shape deformation of the crystal. The second type of strain accounts for the (local) inhomogeneous part of the displacement field and it does not produce any macroscopic effects. A general static displacement $\boldsymbol{u}_R$ can therefore be written as

$$\boldsymbol{u}_R = \boldsymbol{\varepsilon}\boldsymbol{R} + \boldsymbol{v}_R, \tag{12}$$

where $\boldsymbol{\varepsilon}$ is a tensor associated with a homogeneous distortion and the inhomogeneous displacement field $\boldsymbol{v}_R$ is defined so as to vanish at the crystal boundary [8].

The (mechanical) equilibrium state of E_{strain} can be expressed as follows:

$$E^{\text{eq}}_{\text{strain}} = -\tfrac{1}{2}\sum_{R_i,R_j}\boldsymbol{\varphi}^{(2)}_{R_j,R_i}\boldsymbol{u}_{R_i}\sigma_{R_j} - \tfrac{1}{2}\sum_{R_i,R_j,R_k}\boldsymbol{\varphi}^{(3)}_{R_k,R_j,R_i}\boldsymbol{u}_{R_i}\sigma_{R_j}\sigma_{R_k}, \tag{13}$$

which can be used together with equation (12) to obtain the averaged homogeneous and inhomogeneous contributions to the strain-induced energy:

$$\langle E^{\text{H}}_{\text{strain}}\rangle = -\frac{c\varepsilon}{2}\sum_{R_i,R_j}\varphi^{(2)}_{R_j,R_i}|\boldsymbol{R}_j-\boldsymbol{R}_i| - \frac{\varepsilon}{2}\sum_{R_i,R_j,R_k}\varphi^{(3)}_{R_k,R_j,R_i}|\boldsymbol{R}_j-\boldsymbol{R}_i|\langle\sigma_{R_j}\sigma_{R_k}\rangle, \tag{14a}$$

$$\langle E^{\text{I}}_{\text{strain}}\rangle = -\frac{c}{2}\sum_{R_i,R_j}\boldsymbol{\varphi}^{(2)}_{R_j,R_i}\boldsymbol{v}_{R_i} - \tfrac{1}{2}\sum_{R_i,R_j,R_k}\boldsymbol{\varphi}^{(3)}_{R_k,R_j,R_i}\boldsymbol{v}_{R_i}\langle\sigma_{R_j}\sigma_{R_k}\rangle, \tag{14b}$$

where c is the atomic concentration. Note that $E^{\mathrm{H}}_{\mathrm{strain}}$ offers a connection with classical elasticity theory [8], since

$$\langle E^{\mathrm{H}}_{\mathrm{strain}}\rangle = -\tfrac{3}{2}N\Omega\varepsilon^2(C_{11}+2C_{12}) \tag{15}$$

for a cubic disordered alloy system with elastic constants C_{11} and C_{12}, and unit-cell volume Ω. The concentration dependence of equation (15) becomes apparent in combination with equation (14*a*), then

$$3\Omega\varepsilon(C_{11}+2C_{12}) = c\sum_{\boldsymbol{R}_i,\boldsymbol{R}_j}\varphi^{(2)}_{\boldsymbol{R}_j,\boldsymbol{R}_i}|\boldsymbol{R}_j-\boldsymbol{R}_i| + \sum_{\boldsymbol{R}_i,\boldsymbol{R}_j,\boldsymbol{R}_k}\varphi^{(3)}_{\boldsymbol{R}_k,\boldsymbol{R}_j,\boldsymbol{R}_i}|\boldsymbol{R}_j-\boldsymbol{R}_i|\langle\sigma_{\boldsymbol{R}_j}\sigma_{\boldsymbol{R}_k}\rangle. \tag{16}$$

For a cubic crystal, ε is proportional to the lattice constant. The first term in the right-hand side of equation (16) is the well-known Vegard's law, i.e., the linear dependence of the lattice constant with the atomic concentration associated with pairwise Kanzaki forces. The second term of equation (16) accounts for the many-body corrections responsible for the deviations of Vegard's law.

2.3. Strain-induced interactions in reciprocal space

The long-range nature of the elastic interactions is better represented in reciprocal space. For this, we cast the strain-induced energy of equation (9) into reciprocal space using a Fourier transform:

$$E_{\mathrm{strain}} = \frac{1}{2N}\sum_{\boldsymbol{k}}\boldsymbol{u}^{\mathrm{T}}_{\boldsymbol{k}}\boldsymbol{\Phi}^{(0)}_{\boldsymbol{k}}\boldsymbol{u}^{*}_{\boldsymbol{k}} - \frac{1}{N}\sum_{\boldsymbol{k}}\boldsymbol{\varphi}^{(2)}_{\boldsymbol{k}}\boldsymbol{u}_{\boldsymbol{k}}\sigma^{*}_{\boldsymbol{k}} - \frac{1}{N^2}\sum_{\boldsymbol{k},\boldsymbol{q}}\boldsymbol{\varphi}^{(3)}_{\boldsymbol{k},\boldsymbol{q}}\boldsymbol{u}_{\boldsymbol{k}}\sigma_{\boldsymbol{q}}\sigma^{*}_{\boldsymbol{k}+\boldsymbol{q}}, \tag{17}$$

where the sums are over the first Brillouin zone (the exact form of the Fourier components of the two-and three-body Kanzaki forces can be found in the appendix). From the equilibrium condition of E_{strain} with respect to the atomic displacements $\boldsymbol{u}_{\boldsymbol{k}}$, we find

$$\boldsymbol{\Phi}^{(0)}_{\boldsymbol{k}}\boldsymbol{u}^{*}_{\boldsymbol{k}} = \boldsymbol{\varphi}^{(2)}_{\boldsymbol{k}}\sigma^{*}_{\boldsymbol{k}} + \frac{1}{N}\sum_{\boldsymbol{q}}\boldsymbol{\varphi}^{(3)}_{\boldsymbol{k},\boldsymbol{q}}\sigma_{\boldsymbol{q}}\sigma^{*}_{\boldsymbol{k}+\boldsymbol{q}}, \tag{18}$$

which allows us to determine the equilibrium state of the strain-induced energy

$$E^{\mathrm{eq}}_{\mathrm{strain}} = -\frac{1}{2N}\sum_{\boldsymbol{k}}\boldsymbol{\varphi}^{(2)}_{\boldsymbol{k}}\boldsymbol{u}_{\boldsymbol{k}}\sigma^{*}_{\boldsymbol{k}} - \frac{1}{2N^2}\sum_{\boldsymbol{k},\boldsymbol{q}}\boldsymbol{\varphi}^{(3)}_{\boldsymbol{k},\boldsymbol{q}}\boldsymbol{u}_{\boldsymbol{k}}\sigma_{\boldsymbol{q}}\sigma^{*}_{\boldsymbol{k}+\boldsymbol{q}}. \tag{19}$$

By introducing the lattice Green's function $G_{\boldsymbol{k}}$ [25],

$$\boldsymbol{\Phi}^{(0)}_{\boldsymbol{k}}G_{\boldsymbol{k}} = \boldsymbol{I}(1-\delta_{\boldsymbol{k},0}), \tag{20}$$

where $\boldsymbol{I}$ is the identity matrix and $\delta_{\boldsymbol{k},0}$ is the Kronecker delta function. The Fourier transform of the atomic displacements associated with the inhomogeneous relaxations ($\boldsymbol{k}\neq 0$) can be represented as:

$$\boldsymbol{u}_{\boldsymbol{k}} = G^{*}_{\boldsymbol{k}}\boldsymbol{\varphi}^{(2)*}_{\boldsymbol{k}}\sigma_{\boldsymbol{k}} + \frac{1}{N}\sum_{\boldsymbol{q}}G^{*}_{\boldsymbol{k}}\boldsymbol{\varphi}^{(3)*}_{\boldsymbol{k},\boldsymbol{q}}\sigma^{*}_{\boldsymbol{q}}\sigma_{\boldsymbol{k}+\boldsymbol{q}}. \tag{21}$$

Combining equations (21) and (19), the averaged inhomogeneous strain energy can be written in terms of the Fourier components of the many-body strain-induced interactions as follows:

$$\langle E^{\mathrm{I}}_{\mathrm{strain}}\rangle = -cQ + \frac{1}{N}\sum_{\boldsymbol{k}}V^{(2)}_{\boldsymbol{k}}\langle\sigma_{\boldsymbol{k}}\sigma^{*}_{\boldsymbol{k}}\rangle + \frac{1}{N^2}\sum_{\boldsymbol{k},\boldsymbol{q}}V^{(3)}_{\boldsymbol{k},\boldsymbol{q}}\langle\sigma_{\boldsymbol{k}}\sigma_{\boldsymbol{q}}\sigma^{*}_{\boldsymbol{k}+\boldsymbol{q}}\rangle + \frac{1}{N^3}\sum_{\boldsymbol{k},\boldsymbol{q},\boldsymbol{q}'}V^{(4)}_{\boldsymbol{k},\boldsymbol{q},\boldsymbol{q}'}\langle\sigma_{\boldsymbol{k}+\boldsymbol{q}'}\sigma^{*}_{\boldsymbol{q}'}\sigma_{\boldsymbol{q}}\sigma^{*}_{\boldsymbol{k}+\boldsymbol{q}}\rangle, \tag{22}$$

where

$$V^{(2)}_{\boldsymbol{k}} = -\tfrac{1}{2}\boldsymbol{\varphi}^{(2)\mathrm{T}}_{\boldsymbol{k}}G^{*}_{\boldsymbol{k}}\boldsymbol{\varphi}^{(2)*}_{\boldsymbol{k}} + Q, \tag{23*a*}$$

$$V^{(3)}_{\boldsymbol{k},\boldsymbol{q}} = -\boldsymbol{\varphi}^{(3)\mathrm{T}}_{\boldsymbol{k},\boldsymbol{q}}G^{*}_{\boldsymbol{k}}\boldsymbol{\varphi}^{(2)*}_{\boldsymbol{k}}, \tag{23*b*}$$

$$V^{(4)}_{\boldsymbol{k},\boldsymbol{q},\boldsymbol{q}'} = -\tfrac{1}{2}\boldsymbol{\varphi}^{(3)\mathrm{T}}_{\boldsymbol{k},\boldsymbol{q}}G^{*}_{\boldsymbol{k}}\boldsymbol{\varphi}^{(3)*}_{\boldsymbol{k},\boldsymbol{q}'}, \tag{23*c*}$$

are the Fourier components of the two-, three-, and four-body strain-induced interactions, respectively. The real-space self-action correction [8] (i.e., $V^{(2)}_{\boldsymbol{R}_j-\boldsymbol{R}_i=0}\equiv 0$) is introduced in the two-body interactions $V^{(2)}_{\boldsymbol{k}}$ as

$$Q = \frac{1}{2N}\sum_{\boldsymbol{k}}\boldsymbol{\varphi}^{(2)\mathrm{T}}_{\boldsymbol{k}}G^{*}_{\boldsymbol{k}}\boldsymbol{\varphi}^{(2)*}_{\boldsymbol{k}}. \tag{24}$$

The many-body strain-induced interactions have some characteristics that deserve discussion. First, the three-body strain-induced interaction, equation (23*b*), does not satisfy the invariance condition for the exchange of wavevectors $\boldsymbol{k}$ and $\boldsymbol{q}$ in contrast to the three-body interaction introduced within the lattice gas model [27, 28]. Additionally, in the case of the four-body strain-induced interaction the combination of indexes in the product $\sigma_{\boldsymbol{k}+\boldsymbol{q}'}\sigma^{*}_{\boldsymbol{q}'}\sigma_{\boldsymbol{q}}\sigma^{*}_{\boldsymbol{k}+\boldsymbol{q}}$ in equation (22) does not follow the standard combination obtained within the lattice gas model.

3. First-principles parametrization of many-body Kanzaki forces in Cu_3Au

3.1. Computational details

The *ab initio* calculations of the unrelaxed and fully relaxed energies for Cu_3Au alloys were performed using a mixed-basis plane-wave pseudopotential (MBPP) implementation as encoded in the Stuttgart package [29]. The MBPP code is particularly well suited for describing the electronic properties of metallic alloys, since the approach successfully combines the merits of plane-wave pseudopotential methods with an atomic-like basis. This characteristic makes the MBPP computationally efficient, requiring only a few plane waves to achieve converged results. For our present calculations of Cu, Au and their alloys, we have used a 270 eV plane-wave energy cut-off and five local orbitals of d character per atom. The local orbitals were constructed by trimming the atomic pseudowave function beyond a cut-off radius of 2.10 and 2.25 au for Cu and Au atoms, respectively. This radius was chosen to allow for structural relaxations in Cu–Au alloys. Valence electrons were represented by norm-conserving, nonlocal pseudopotentials.

In all the calculations, a local density approximation (LDA) to the exchange and correlation energy as proposed by Ceperley and Alder [30] was used. The electron densities

were calculated in a Fourier representation enclosing plane waves up to 410 eV. The k-point mesh integration was done using a special set of points as provided by the Moreno–Soler scheme [31] together with a Gaussian broadening of 0.1 eV. Using an equivalent set of k points guarantees the best possible cancellation of errors when computing energy difference between isostructural compounds. In addition, its has been shown that equivalent k-point convergence is faster than absolute convergence [32]. A grid of $12 \times 12 \times 12$ k points for the simple cubic $L1_2$ unit cell was used in all calculations or denser when this k-point mesh was incommensurate with the periodicity of the structure. With the above parameters, relative energies (with respect to the $L1_2$ structure) were numerically converged to within 1 meV/atom. To test LDA accuracy, we also carried out calculations within the generalized-gradient approximation in the Perdew–Burke–Ernzerhof parametrization [33] for selected structures; and qualitatively we found the same trends as in the LDA data.

For the dynamical matrix $\mathbf{\Phi}^{(0)}$, we have used the expression suggested by Krivoglaz (fcc lattices) [15]:

$$\Phi^{(0)}_{\boldsymbol{k},xx} = aC_{11}\big(2 - \cos(ak_x/2)[\cos(ak_y/2) + \cos(ak_z/2)]\big) + a(2C_{44} - C_{11})[1 - \cos(ak_y/2)\cos(ak_z/2)], \quad (25a)$$

$$\Phi^{(0)}_{\boldsymbol{k},xy} = a(2C_{12} - C_{44})\sin(ak_x/2)\sin(ak_y/2), \quad (25b)$$

where a represents the lattice constant and C_{11}, C_{12}, C_{44} are the elastic constants. The other components of the dynamical matrix are obtained by cyclic permutation of indices. It is possible to keep the parametrization of the strain-induced interactions within first principles by calculating the dynamical matrix using, for example, a density-functional perturbation theory [34]. However, for the sake of simplicity, we have used expression (25) to parametrize the dynamical matrix. This choice can be justified for close-packed lattices as the phonon spectra are easy to reproduce with rather simple models—as opposed to body-centred cubic materials where phonon softening plays a subtle and complicated role. We have compared the phonon spectrum predicted by equation (25) with the experimental data [35] with rather good agreement. For such comparison, we used our calculated LDA values for the lattice constant $a = 3.7$ Å and the elastic constants (i.e., $C_{11} = 238$, $C_{12} = 159$, $C_{44} = 87$ GPa) for Cu_3Au in the $L1_2$ phase.

3.2. Structure selection

The structure selection was directed by the Lifshitz theorem, which states that every periodic function in the reciprocal space exhibits extrema at the high symmetry points. Structures at high symmetry lines are also of particular importance, since structural instabilities and main features of the phase diagrams are determined by the extrema of the reciprocal-space interactions (Landau theory) [36]. Our set of input structures contains three Lifshitz structures (i.e., $L1_2$, $D0_{22}$, $CuPt_3$-like) and 13 special structures along the high symmetry [100], [110], [111] directions and between the X and W points in the Brillouin zone [36]. The spacing between [100] and [110] superlattice structures along the same line is $\frac{1}{4}$ reciprocal-lattice units. Superlattice structures along the [111] direction are spaced $\frac{1}{8}$ reciprocal-lattice units (see figure 2). For example, structures with Cu_3Au periodicity along the [100], [110], [111] directions are denoted by Z_1, Y_1, and V_1, respectively [37]. Superlattice structures with Cu_6Au_2 periodicity are denoted as Γ–X_1, Γ–K_1, and Γ–L_1, respectively for the [100], [110], [111] directions. The same nomenclature applies for the $Cu_5AuCuAu$ (Γ–X_2, Γ–K_2, Γ–L_2) and Cu_4AuCu_2Au (Γ–X_3, Γ–K_3, Γ–L_3) superlattice structures. All structures have been studied previously in the literature and their crystallographic information is available elsewhere [3, 8, 36, 37].

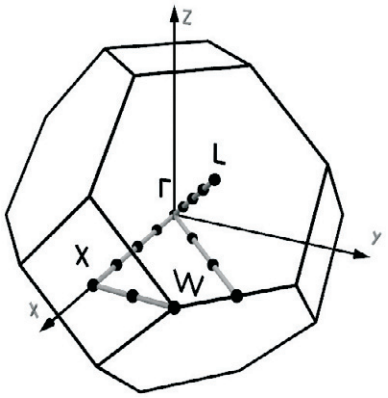

Figure 2. First Brillouin zone for a face-centred lattice. Ordered and superlattice structures used in the first-principles calculations were selected along high symmetry directions, i.e., [100], [110], [111] and along the lines connecting the X and W points on the edge of the zone. The spacing between the structures along each line is $\frac{1}{4}$ reciprocal-lattice units. Structures along the Γ–L direction are spaced $\frac{1}{8}$ reciprocal-lattice units (cf table 1).

We used the MBPP method to calculate the total energy of the 16 fcc-based $Cu_{3n}Au_n$ ordered structures described above. For the fully relaxed calculations, all the crystal parameters were optimized, either by minimizing the total energy against the proper distortion, e.g., volume or the c/a ratio, and by minimizing the forces on the atoms with positions not fixed by symmetry. The atomic positions were relaxed using the Broyden–Fletcher–Goldfarb–Shanno method [38], achieving an accuracy of 3 meV $Å^{-1}$. Table 1 summarizes the results of the calculations.

3.3. Homogeneous and inhomogeneous contributions to the strain energy

Using the theory developed in section 2, we have expanded the strain-induced energy of Cu_3Au alloys in terms of many-body Kanzaki forces with respect to the $L1_2$ ground state (chemical reference state). In this way, we focused only on the strain-induced energy without losing any generality. The chemical part of the alloy energy can be described in a straightforward manner by cluster expanding the unrelaxed energies in terms of concentration-independent interactions.

We have assessed the quality of the expansion by systematically including many-body Kanzaki forces as a function of the distance. In all cases, we observed that the Kanzaki forces converged very quickly with distance and number of points in the cluster figures, e.g., clusters involving

Table 1. Relaxation energy ΔE_{DFT} (in meV/atom) for fcc-based ordered Cu–Au compounds as calculated with the MBPP using the LDA for the xc potential. DFT energy for each structure is quoted relative to its strained state with the $L1_2$ lattice constant. The inhomogeneous part to the strain-induced energy has been split into the pairwise $\langle E^{\mathrm{I(2)}}_{\mathrm{strain}}\rangle$ and three plus four-body $\langle E^{\mathrm{I(3+4)}}_{\mathrm{strain}}\rangle$ contributions (see footnote 4). The last column stands for the fitting error for each individual structure. The root mean squared error for the entire set is 4 meV/atom. See [3, 8], and [36] for a detailed crystallographic description of the different ordered and superlattice structures.

Structure	ΔE_{DFT}	$\langle E^{\mathrm{I(2)}}_{\mathrm{strain}}\rangle$	$\langle E^{\mathrm{I(3+4)}}_{\mathrm{strain}}\rangle$	$\langle E^{\mathrm{H}}_{\mathrm{strain}}\rangle$	Error
$L1_2$	0.0	0.0	0.0	0.0	0.0
$D0_{22}$	0.1	0.0	0.0	0.0	0.1
$CuPt_3$	−1.5	0.0	0.0	−1.7	−0.2
Y_1	−74.1	−71.3	0.8	−3.4	0.2
Γ–X_1	−177.8	−151.9	−23.4	−6.8	−4.3
Γ–X_2	−76.4	−76.0	1.2	−3.4	−1.8
Γ–X_3	−73.9	−71.4	0.8	−3.4	−0.1
Z_1	−28.7	−26.1	0.3	−1.7	1.2
Γ–K_1	−112.6	−93.6	−8.1	−5.1	5.8
Γ–K_2	−59.9	−47.4	−1.1	−2.6	8.8
Γ–K_3	−30.3	−27.4	0.4	−1.7	1.6
V_1	−68.3	−64.5	2.3	−5.1	1.0
Γ–L_1	−157.5	−128.4	−14.4	−7.6	7.1
Γ–L_2	−60.6	−64.2	2.2	−5.1	−6.5
Γ–L_3	−62.3	−64.5	2.3	−5.1	−5.0
$D0_{23}$	0.1	−0.2	0.0	0.0	−0.1

Table 2. Two- and three-body Kanzaki forces in meV Å^{-1} for the Cu_3Au alloy system.

Two-body	Three-body
$\varphi^{(2)}_1 = 627.0$	$\varphi^{(3)}_1 = 88.7$
$\varphi^{(2)}_2 = 61.3$	$\varphi^{(3)}_2 = -3.5$
$\varphi^{(2)}_3 = -1.4$	$\varphi^{(3)}_3 = -8.3$
	$\varphi^{(3)}_4 = 9.5$

atoms in the fourth coordination shell have Kanzaki forces of the order 10 meV Å^{-1} (see table 2). A precise expansion for Cu_3Au includes three pairwise and four three-body Kanzaki forces (cf figure 3 and table 2)[3].

We have split the strain-induced energy of all the input $Cu_{3n}Au_n$ structures into their homogeneous ($\boldsymbol{k} = 0$) and inhomogeneous ($\boldsymbol{k} \neq 0$) contributions. Previous attempts to describe the elastic interactions in binary alloys treated the homogeneous contribution as independent of the configurational degrees of freedom [1, 8, 9]. In general, this is not the case, as can be seen in equation (14*a*). Interestingly enough, $\langle E^{\mathrm{H}}_{\mathrm{strain}}\rangle$ is not the most important contribution to the alloy strain-induced energy in Cu_3Au. This can be appreciated in table 1, where the homogeneous part of $\langle E_{\mathrm{strain}}\rangle$ is displayed in the fifth column. For all the structures considered here, $\langle E^{\mathrm{H}}_{\mathrm{strain}}\rangle$ is less than 8 meV/atom and usually represents only a minor fraction of E_{strain}. Exceptions appear for structures without internal atomic degrees of freedom, such as the $CuPt_3$-type structure, where the homogeneous part constitutes the only contribution to the strain-induced energy.

[3] The use of cross-validatory approaches [39] and large input databases could produce slightly different results. However, due to the nature of the forces (and interactions) involved in the strain-induced energy, we are convinced that only quantitative but not qualitative differences will arise in that case. In order to illustrate the use of the theory, our selected input database and cluster figures should be accurate enough.

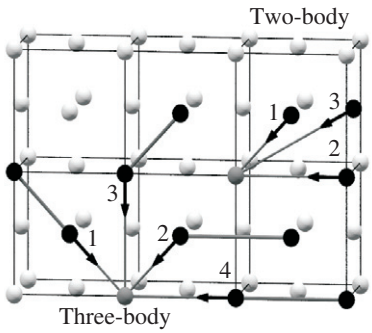

Figure 3. Pair and three-body cluster figures used in the calculation of the many-body Kanzaki forces.

The main contribution to the strain-induced energy comes from the inhomogeneous part $\langle E^{\mathrm{I}}_{\mathrm{strain}}\rangle$. In table 1, we have decomposed the inhomogeneous part into the pair $\langle E^{\mathrm{I(2)}}_{\mathrm{strain}}\rangle$ and many-body (three plus four-body) $\langle E^{\mathrm{I(3+4)}}_{\mathrm{strain}}\rangle$ contributions. As expected, in all cases the many-body contribution is smaller than the pairwise contribution[4]. $\langle E^{\mathrm{I(3+4)}}_{\mathrm{strain}}\rangle$ is very small for structures Z_1, Y_1, and V_1; that is, for short-period A_3B-superlattice structures in the [100], [110], and [111] directions, respectively. The opposite occurs for the Cu_6Au_2 long-period structures along the same directions: for the structures Γ–X_1, Γ–K_1 and Γ–L_1, ∼95% of strain-induced energy originates from the inhomogeneous part. In other words, the latter structures correspond to wavevectors located along high symmetry lines in the neighbourhood of the Γ point (see figure 2).

An analysis of the atomic arrangements in the three-body cluster figures (figure 3) together with the Kanzaki forces reported in table 2 shows that three-body Kanzaki forces corresponding to in-line atomic arrangements are the most important ones (e.g., three-body cluster figures 1 and 4 in figure 3).

3.4. Fourier analysis of the strain-induced interactions

In figure 4, we show the main strain-induced interactions associated with the Kanzaki forces (cf table 2 and figure 3). Note that the two-body strain-induced interaction of Cu_3Au shows a rather simple structure everywhere but at the Γ point. This is also true for the three-body interactions that are non-analytic for all fixed wavevectors $\boldsymbol{q}_0$ (in figure 4(b), we show the dispersion curves for the three-body strain-induced interaction for $\boldsymbol{q}_0$ at the high symmetry points Γ, X, W, and L).

One can analyse the impact of approximating a non-analytical function such as $V^{(2)}_{\boldsymbol{k}}$ by a finite number of real-space terms—as often occurs in concentration-independent cluster expansions—by monitoring the behaviour of

$$V^{(2)}_{\boldsymbol{k}} = \sum_{i=1}^{n} V^{(2)}_{\boldsymbol{R}_i} \exp(\mathrm{i}\boldsymbol{k}\cdot\boldsymbol{R}_i), \tag{26}$$

[4] For Cu_3Au, four-body interactions are at least one order of magnitude smaller than the three-body interactions.

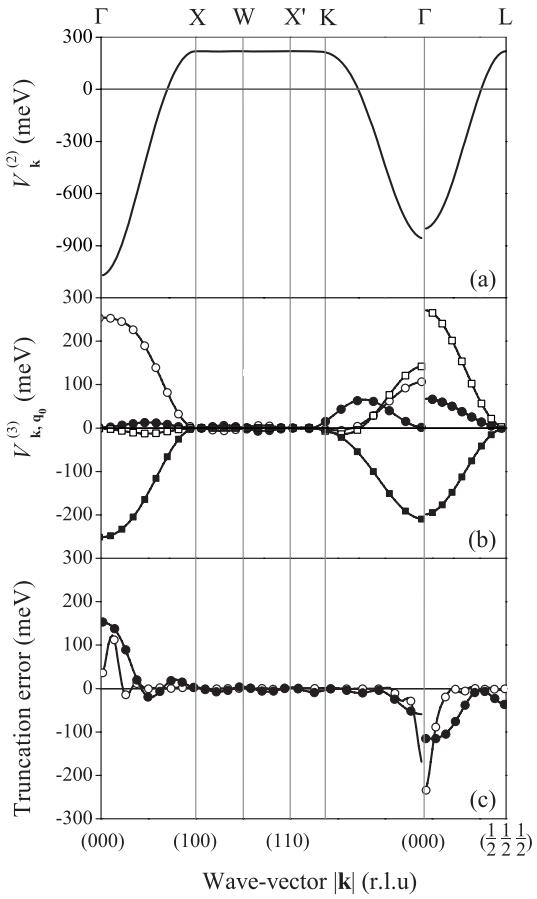

Figure 4. Fourier component of (a) two-body and (b) three-body strain-induced interactions. The dispersion curves of all interactions display a non-analytic behaviour around the Γ point for the two-body interactions and for fixed values of the wavevector $\boldsymbol{q}_0$ (=X (open circles), W (filled circles), L (open squares), and Γ (filled squares)) for the three-body interactions. (c) Truncation error for a real-space expansion of the strain-induced interactions (cf equation (26)) using 10 coordination shells (filled circles) and 100 coordination shells (open circles). Note that the error peaks at the Γ point but extends far in the Brillouin zone, e.g., all the way along the Γ–X, Γ–L, and Γ–K directions (cf figure 2).

i.e., the Fourier expansion of $V^{(2)}_{\boldsymbol{k}}$, as a function of the number of terms n. In figure 4(c) we have plotted the residuals of the expansion (26) for $n = 10$ and 100. Notice that even for a large number of terms ($n = 100$), the expansion has an error of ∼100–150 meV in the vicinity of the Γ point. This truncation error decreases slowly as the number of terms in the real-space expansion increases. This can be crucial in the case of phase-separating systems, where the structure formation is dominated by the long-wave interactions (i.e., $\boldsymbol{k}, \boldsymbol{q} \to \Gamma$).

4. Summary and conclusions

We have developed a perturbative approach to the strain-induced effects in binary alloys. In the theory, the strain-induced energy is expressed in terms of many-body Kanzaki forces that are coupled to the many-body atomic correlation functions. The conceptual simplicity of our approach allows the use of state-of-the-art *ab initio* calculations to determine effective elastic many-body interactions.

In praxis, the strain-induced energy is expanded with respect to a given unrelaxed (chemical) state, e.g., the $L1_2$ in a A_3B fcc-based alloy. The Kanzaki force parameters are determined by fitting E_{strain} to the energy of a set of structures consistent with the reference-state concentration. Since the strain-induced energy is long-ranged, sensitive choices for the input structures are superlattice structures with varying periodicities along the main crystallographic directions. A cluster expansion of the unrelaxed reference state will render concentration-independent effective cluster interactions with good convergence properties. In this way, a complete *ab initio* parametrization of the alloy energy can be achieved.

We have applied the theory and the above procedure to Cu_3Au alloys. On the basis of LDA first-principles calculations, we found that the Kanzaki forces exhibit fast convergence with the interatomic distance and number of points in the associated cluster figures. The many-body contributions to the relaxation energy, however, strongly depend on the local atomic environment. Structures with pure-Au neighbouring layers display the most pronounced many-body elastic effects.

We have found that the dominant contribution to the strain-induced energy of Cu_3Au originates from the inhomogeneous distortions, that is, from the local displacement field $\boldsymbol{v}_R$. Less than 5% of the elastic energy of Cu_3Au is associated with the uniform static displacement field that is responsible, in turn, for the (macroscopic) changes of the crystal shape. Moreover, our results show that the homogeneous part of the strain-induced energy is barely sensitive to the state of order in Cu–25 at.% Au compounds. All these facts together provide a first-principles explanation of an intriguing and long-standing experimental observation. Cu_3Au undergoes a first-order transition from the ordered $L1_2$ to the disordered fcc structure at 660 K. X-ray measurements in Cu_3Au alloys have shown that the lattice parameter is virtually constant across the order–disorder transition, regardless the large atomic size mismatch between Cu and Au [40].

We have investigated the dispersion curves of the resulting strain-induced interactions in Cu_3Au. Our analysis showed that two-body $V^{(2)}_{\boldsymbol{k}}$ interactions are non-analytical at the point $k = \Gamma$. This is also true for the three-body $V^{(3)}_{\boldsymbol{k},\boldsymbol{q}}$ interactions that are discontinuous for every fixed wavevector $\boldsymbol{q}_0$. Therefore, a real-space expansion of the strain-induced interactions necessarily provides an incomplete description, not only at the Γ-point itself but also far in the Brillouin zone (e.g., all the way to the X, L, and K points at the zone boundary). In other words, a real-space expansion of the strain-induced interactions in Cu_3Au smears out the non-analyticity around the Γ point (this can be observed even for cluster expansions with concentration-independent effective cluster interactions involving 100 coordination shells).

An analysis of the alloy configurational and elastic interactions in terms of Kanzaki forces renders a set of parameters with an immediate physical meaning. Consequently, a Kanzaki force expansion has a convergence radius (i.e., forces associated with compact cluster figures dominate over the long-ranged cluster figures with many vertices), in contrast to the

concentration-independent cluster expansion. The many-body strain-induced interactions can be used together with statistical mechanics models in the description of thermodynamic and structural properties of atomic size mismatch systems [41]. Finally, the developed theory can be fully *ab initio* if the dynamical matrix is calculated using density-functional perturbation theory.

Acknowledgments

We are grateful to Professor Mark Asta and Dr Ayse Turak for critically reading the manuscript. One of us (AD-O) is pleased to acknowledge the support from the Alexander von Humboldt Foundation.

Appendix. Fourier components of two- and three-body Kanzaki forces

The strain-induced energy is expressed in terms of the many-body Kanzaki forces. In their reciprocal-space form, these many-body forces can be expressed in terms of the lattice constant a and the components of the wavevector $\boldsymbol{k}$ as follows:

$$\boldsymbol{\varphi}_1^{(2)}(\mathbf{k}) = -\mathrm{i}2\sqrt{2}\varphi_1^{(2)} \times \left\| \begin{array}{c} \left[\cos(\frac{a}{2}k_y) + \cos(\frac{a}{2}k_z)\right]\sin(\frac{a}{2}k_x) \\ \left[\cos(\frac{a}{2}k_x) + \cos(\frac{a}{2}k_z)\right]\sin(\frac{a}{2}k_y) \\ \left[\cos(\frac{a}{2}k_x) + \cos(\frac{a}{2}k_y)\right]\sin(\frac{a}{2}k_z) \end{array} \right\|, \tag{A.1}$$

$$\boldsymbol{\varphi}_2^{(2)}(\mathbf{k}) = -\mathrm{i}2\varphi_2^{(2)} \left\| \begin{array}{c} \sin(ak_x) \\ \sin(ak_y) \\ \sin(ak_z) \end{array} \right\|, \tag{A.2}$$

$$\boldsymbol{\varphi}_3^{(2)}(\mathbf{k}) = -\mathrm{i}\sqrt{\frac{2}{3}}\varphi_3^{(2)} \times \left\| \begin{array}{c} \left\{ \begin{array}{l} \sin\left[\frac{a}{2}(k_x-k_y-2k_z)\right] + \sin\left[\frac{a}{2}(k_x+k_y-2k_z)\right] + \\ \sin\left[\frac{a}{2}(k_x-2k_y-k_z)\right] + 2\sin\left[\frac{a}{2}(2k_x-k_y-k_z)\right] + \\ 2\sin\left[\frac{a}{2}(2k_x+k_y-k_z)\right] + \sin\left[\frac{a}{2}(k_x+2k_y-k_z)\right] + \\ \sin\left[\frac{a}{2}(k_x-2k_y+k_z)\right] + 2\sin\left[\frac{a}{2}(2k_x-k_y+k_z)\right] + \\ 2\sin\left[\frac{a}{2}(2k_x+k_y+k_z)\right] + \sin\left[\frac{a}{2}(k_x+2k_y+k_z)\right] + \\ \sin\left[\frac{a}{2}(k_x-k_y+2k_z)\right] + \sin\left[\frac{a}{2}(k_x+k_y+2k_z)\right] \end{array} \right\} \\ -\left\{ \begin{array}{l} \sin\left[\frac{a}{2}(k_x-k_y-2k_z)\right] - \sin\left[\frac{a}{2}(k_x+k_y-2k_z)\right] + \\ 2\sin\left[\frac{a}{2}(k_x-2k_y-k_z)\right] + \sin\left[\frac{a}{2}(2k_x-k_y-k_z)\right] - \\ \sin\left[\frac{a}{2}(2k_x+k_y-k_z)\right] - 2\sin\left[\frac{a}{2}(k_x+2k_y-k_z)\right] + \\ 2\sin\left[\frac{a}{2}(k_x-2k_y+k_z)\right] + \sin\left[\frac{a}{2}(2k_x-k_y+k_z)\right] - \\ \sin\left[\frac{a}{2}(2k_x+k_y+k_z)\right] - 2\sin\left[\frac{a}{2}(k_x+2k_y+k_z)\right] + \\ \sin\left[\frac{a}{2}(k_x-k_y+2k_z)\right] - \sin\left[\frac{a}{2}(k_x+k_y+2k_z)\right] \end{array} \right\} \\ -\left\{ \begin{array}{l} 2\sin\left[\frac{a}{2}(k_x-k_y-2k_z)\right] + 2\sin\left[\frac{a}{2}(k_x+k_y-2k_z)\right] + \\ \sin\left[\frac{a}{2}(k_x-2k_y-k_z)\right] + \sin\left[\frac{a}{2}(2k_x-k_y-k_z)\right] + \\ \sin\left[\frac{a}{2}(2k_x+k_y-k_z)\right] + \sin\left[\frac{a}{2}(k_x+2k_y-k_z)\right] - \\ \sin\left[\frac{a}{2}(k_x-2k_y+k_z)\right] - \sin\left[\frac{a}{2}(2k_x-k_y+k_z)\right] - \\ \sin\left[\frac{a}{2}(2k_x+k_y+k_z)\right] - \sin\left[\frac{a}{2}(k_x+2k_y+k_z)\right] - \\ 2\sin\left[\frac{a}{2}(k_x-k_y+2k_z)\right] - 2\sin\left[\frac{a}{2}(k_x+k_y+2k_z)\right] \end{array} \right\} \end{array} \right\|, \tag{A.3}$$

$$\boldsymbol{\varphi}_1^{(3)}(\mathbf{k},\mathbf{q}) = -\mathrm{i}\sqrt{2}\varphi_1^{(3)} \times \left\| \begin{array}{l} \left\{ \begin{array}{l} \sin\left[\frac{a}{2}(k_x-q_x+k_y-q_y)\right] + \\ \sin\left[\frac{a}{2}(k_x-q_x-k_y+q_y)\right] + \\ \sin\left[\frac{a}{2}(k_x-q_x+k_z-q_z)\right] + \\ \sin\left[\frac{a}{2}(k_x-q_x-k_z+q_z)\right] \end{array} \right\} \\ \left\{ \begin{array}{l} \sin\left[\frac{a}{2}(k_x-q_x+k_y-q_y)\right] - \\ \sin\left[\frac{a}{2}(k_x-q_x-k_y+q_y)\right] + \\ \sin\left[\frac{a}{2}(k_y-q_y+k_z-q_z)\right] + \\ \sin\left[\frac{a}{2}(k_y-q_y-k_z+q_z)\right] \end{array} \right\} \\ \left\{ \begin{array}{l} \sin\left[\frac{a}{2}(k_x-q_x+k_z-q_z)\right] + \\ \sin\left[\frac{a}{2}(k_y-q_y+k_z-q_z)\right] - \\ \sin\left[\frac{a}{2}(k_x-q_x-k_z+q_z)\right] - \\ \sin\left[\frac{a}{2}(k_y-q_y-k_z+q_z)\right] \end{array} \right\} \end{array} \right\| \tag{A.4}$$

$$\boldsymbol{\varphi}_2^{(3)}(\mathbf{k},\mathbf{q}) = -\mathrm{i}\sqrt{2}\varphi_2^{(3)} \times \left\| \begin{array}{l} \left\{ \begin{array}{l} \sin\left[\frac{a}{2}(k_x-2q_x-k_y)\right] + \sin\left[\frac{a}{2}(k_x-2q_x+k_y)\right] + \\ \sin\left[\frac{a}{2}(k_x+k_y-2q_y)\right] + \sin\left[\frac{a}{2}(k_x-k_y+2q_y)\right] + \\ \sin\left[\frac{a}{2}(k_x-2q_x-k_z)\right] + \sin\left[\frac{a}{2}(k_x-2q_x+k_z)\right] + \\ \sin\left[\frac{a}{2}(k_x+k_z-2q_z)\right] + \sin\left[\frac{a}{2}(k_x-k_z+2q_z)\right] \end{array} \right\} \\ -\left\{ \begin{array}{l} \sin\left[\frac{a}{2}(k_x-2q_x-k_y)\right] - \sin\left[\frac{a}{2}(k_x-2q_x+k_y)\right] - \\ \sin\left[\frac{a}{2}(k_x+k_y-2q_y)\right] + \sin\left[\frac{a}{2}(k_x-k_y+2q_y)\right] - \\ \sin\left[\frac{a}{2}(k_y-2q_y-k_z)\right] - \sin\left[\frac{a}{2}(k_y-2q_y+k_z)\right] - \\ \sin\left[\frac{a}{2}(k_y+k_z-2q_z)\right] - \sin\left[\frac{a}{2}(k_y-k_z-2q_z)\right] \end{array} \right\} \\ -\left\{ \begin{array}{l} \sin\left[\frac{a}{2}(k_x-2q_x-k_z)\right] + \sin\left[\frac{a}{2}(k_y-2q_y-k_z)\right] - \\ \sin\left[\frac{a}{2}(k_x-2q_x+k_z)\right] - \sin\left[\frac{a}{2}(k_y-2q_y+k_z)\right] - \\ \sin\left[\frac{a}{2}(k_x-k_z-2q_z)\right] - \sin\left[\frac{a}{2}(k_y+k_z-2q_z)\right] + \\ \sin\left[\frac{a}{2}(k_x-k_z+2q_z)\right] + \sin\left[\frac{a}{2}(k_y-k_z+2q_z)\right] \end{array} \right\} \end{array} \right\| \tag{A.5}$$

$$\boldsymbol{\varphi}_3^{(3)}(\mathbf{k},\mathbf{q}) = -\mathrm{i}\sqrt{2}\varphi_3^{(3)} \times \left\| \begin{array}{l} \left\{ \begin{array}{l} \sin\left[\frac{a}{2}(2k_x-q_x-q_y)\right] + \sin\left[\frac{a}{2}(2k_x-q_x+q_y)\right] + \\ \sin\left[\frac{a}{2}(2k_x-q_y-q_z)\right] + \sin\left[\frac{a}{2}(2k_x-q_y+q_z)\right] \end{array} \right\} \\ \left\{ \begin{array}{l} \sin\left[\frac{a}{2}(2k_y+q_x-q_y)\right] + \sin\left[\frac{a}{2}(2k_y-q_x-q_y)\right] + \\ \sin\left[\frac{a}{2}(2k_y-q_y-q_z)\right] + \sin\left[\frac{a}{2}(2k_y-q_y+q_z)\right] \end{array} \right\} \\ \left\{ \begin{array}{l} \sin\left[\frac{a}{2}(2k_z+q_x-q_z)\right] + \sin\left[\frac{a}{2}(2k_z+q_y-q_z)\right] + \\ \sin\left[\frac{a}{2}(2k_z-q_x-q_z)\right] + \sin\left[\frac{a}{2}(2k_z-q_y-q_z)\right] \end{array} \right\} \end{array} \right\| \tag{A.6}$$

$$\boldsymbol{\varphi}_4^{(3)}(\mathbf{k},\mathbf{q}) = -\mathrm{i}2\varphi_4^{(3)} \left\| \begin{array}{c} \sin\left[a(k_x-q_x)\right] \\ \sin\left[a(k_y-q_y)\right] \\ \sin\left[a(k_z-q_z)\right] \end{array} \right\|. \tag{A.7}$$

References

[1] Ferreira L G, Mbaye A A and Zunger A 1987 *Phys. Rev.* B **37** 10547
[2] Laks D B, Ferreira L G, Froyen S and Zunger A 1992 *Phys. Rev.* B **46** 12587
[3] Zunger A 1994 *Statics and Dynamics of Alloy Phase Transformations* ed P E A Turchi and A Gonis (New York: Plenum) p 361
[4] Asta M and Foiles S M 1996 *Phys. Rev.* B **53** 2389

[5] Reichert H, Schöps A, Ramsteiner I B, Bugaev V N, Shchyglo O, Udyansky A, Dosch H, Asta M, Drautz R and Honkimäki V 2005 *Phys. Rev. Lett.* **95** 235703
[6] Cook H E and de Fontaine D 1969 *Acta Metall.* **17** 915
Cook H E and de Fontaine D 1971 *Acta Metall.* **19** 607
[7] de Fontaine D 1979 *Solid State Phys.* **34** 73
[8] Khachaturyan A G 1983 *Theory of Structural Transformations in Solids* (New York: Wiley)
[9] de Gironcoli S, Giannozzi P and Baroni S 1991 *Phys. Rev. Lett.* **66** 2116
[10] Beiden S V and Vaks V G 1992 *Phys. Lett.* A **163** 209
Beiden S V, Samolynk G D, Vaks V G and Zein N E 1994 *J. Phys.: Condens. Matter* **6** 8487
[11] Sanchez J M, Ducastelle F and Gratias D 1984 *Physica* A **128** 334
[12] Sanchez J M 1993 *Phys. Rev.* B **48** 14013
[13] de Fontaine D 1994 *Solid State Phys.* **47** 33
[14] Lu Z W, Laks D B, Wei S-H and Zunger A 1994 *Phys. Rev.* B **50** 6642
[15] Krivoglaz M A 1996 *X-Ray and Neutron Diffraction in Nonideal Crystals* (Berlin: Springer)
Krivoglaz M A 1962 *Fiz. Tverd. Tela* **4** 2840
Krivoglaz M A 1967 *Fiz. Tverd. Tela* **9** 2861
[16] Matsubara T 1952 *J. Phys. Soc. Japan* **7** 270
[17] Kanzaki H 1957 *J. Phys. Chem. Solids* **2** 24
Kanzaki H 1966 *Tech. Rep. ISSP* A **232** 14
[18] Blanter M S 1994 *Phys. Status Solidi* b **181** 377
[19] Hoffman D W 1970 *Acta Metall.* **18** 819
[20] Shirley C G 1974 *Phys. Rev.* B **10** 1149
[21] Oates W A and Stoneham A M 1983 *J. Phys. F: Met. Phys.* **13** 2427
[22] Shirley A I and Hall C K 1986 *Phys. Rev.* B **33** 8084
Shirley A I and Hall C K 1986 *Phys. Rev.* B **33** 8099
[23] Belashchenko K D, Pankratov I R, Samolyuk G D and Vaks V G 2002 *J. Phys.: Condens. Matter* **14** 565
[24] Bugaev V N, Reichert H, Shchyglo O, Udyansky A, Sikula Y and Dosch H 2002 *Phys. Rev.* B **65** 180203(R)
[25] Born M and Huang K 1998 *Dynamical Theory of Crystal Lattices* (Oxford: Clarendon)
[26] Khachaturyan A G, Semenovskaya S and Tsakalakos T 1995 *Phys. Rev.* B **52** 15909
[27] Lee T D and Yang C N 1952 *Phys. Rev.* **87** 410
[28] Bugaev V N and Chepulskii R V 1995 *Acta Crystallogr.* A **51** 456
Bugaev V N and Chepulskii R V 1995 *Acta Crystallogr.* A **51** 463
[29] Meyer B, Elsässer C, Lechermann F and Fähnle M, *FORTRAN90 Program for Mixed-Basis Pseudopotential Calculations* (Stuttgart: Max-Planck-Institut für Metallforschung) unpublished
[30] Ceperley D M and Alder B J 1980 *Phys. Rev. Lett.* **45** 566
[31] Moreno J and Soler J M 1992 *Phys. Rev.* B **45** 13891
[32] Froyen S 1989 *Phys. Rev.* B **39** 3168
[33] Perdew J P, Burke K and Ernzerhof M 1996 *Phys. Rev. Lett.* **77** 3865
Perdew J P, Burke K and Ernzerhof M 1997 *Phys. Rev. Lett.* **78** 1396
[34] Baroni S, de Gironcoli S, Dal Corso A and Giannozzi P 2001 *Rev. Mod. Phys.* **73** 515
[35] Katano S, Iizumi M and Noda Y 1988 *J. Phys. F: Met. Phys.* **18** 2195
[36] Shchyglo O, Bugaev V N, Drautz R, Udyansky A, Reichert H and Dosch H 2005 *Phys. Rev.* B **72** 140201(R)
[37] Lu Z W, Wei S-H, Zunger A, Frota-Pessoa S and Ferreira L G 1991 *Phys. Rev.* B **44** 512
[38] Shanno D F and Phua K H 1976 *ACM Trans. Math. Softw.* **2** 87
[39] Stone M 1974 *J. R. Stat. Soc.* B **36** 111
[40] Betteridge W 1949 *J. Inst. Met.* **75** 559
[41] Bugaev V N, Udyansky A, Shchyglo O, Reichert H and Dosch H 2006 *Phys. Rev.* B **74** 024202